Choudhury, Tuhin; Kurvinen, Emil; Viitala, Raine; Sopanen, Jussi

Development and verification of frequency domain solution methods for rotor-bearing system responses caused by rolling element bearing waviness

Published in:
Mechanical Systems and Signal Processing

DOI:
10.1016/j.ymssp.2021.108117

Published: 15/01/2022

Document Version
Publisher's PDF, also known as Version of record

Mechanical Systems and Signal Processing 163 (2022) 108117

Contents lists available at ScienceDirect

Mechanical Systems and Signal Processing

journal homepage: www.elsevier.com/locate/ymssp

Development and verification of frequency domain solution methods for rotor-bearing system responses caused by rolling element bearing waviness

Tuhin Choudhury [a,*], Emil Kurvinen [a], Raine Viitala [b], Jussi Sopanen [a]

[a] Department of Mechanical Engineering, Lappeenranta-Lahti University of Technology LUT, Lappeenranta, Finland
[b] Department of Mechanical Engineering, Aalto University, Espoo, Finland

ARTICLE INFO

Keyword:
Bearing roundness profile
Experimental verification
Frequency domain solution
Linearized stiffness
Rolling Element Bearing
Waviness

ABSTRACT

In rotordynamic simulations, rolling element bearing waviness is often accounted using nonlinear models that are solved with a numerical integration scheme in time domain. This approach generates accurate system response, but the method is limited in terms of computational efficiency. This study proposes two novel methods for solution of the responses caused by the bearing waviness excitation in frequency domain, and compares the result with a previously developed, time domain based numerical simulation. The first method known as Base Excitation Method (BEM) considers the waviness as base excitation whereas the second method, known as Bearing Kinematics Augmented Base Excitation Method (BKA-BEM), utilizes a four degree of freedom, quasi-static model to include the bearing kinematics and refine the base excitations due to waviness. The methods are validated with a test case, in which measured low order waviness components of the bearing inner ring roundness profile were used as source for excitation. The accuracy and robustness of the proposed methods in calculating the subcritical harmonic response frequencies and amplitudes are examined for different roundness profiles. The results show that the proposed methods performed relatively well compared to previously developed, time domain solution based numerical model and experimental results. Furthermore, the frequency domain solutions significantly reduce the computational time which makes them easily applicable to simulation-based transfer learning, iterative inverse problems and optimization solutions.

1. Introduction

The performance of a rotor-bearing system is largely dependent on its dynamic behavior. To successfully design rotor systems, determine manufacturing tolerances and ensure flawless behavior in operating conditions, computationally efficient simulation tools for investigation of system performance are needed. Moreover, in order to design and model a rotating machine accurately, geometrical imperfections such as variations in the roundness profiles of circular components and their effects on machine performance should be accounted for. Such imperfections cause excitations, which then cause unwanted vibration in the system, leading to unpredictable dynamic responses during operation.

In rotating machines, geometric imperfections in the bearing components cause undesired relative displacement between the

* Corresponding author.
E-mail address: Tuhin.Choudhury@lut.fi (T. Choudhury).

https://doi.org/10.1016/j.ymssp.2021.108117
Received 20 January 2021; Received in revised form 1 May 2021; Accepted 3 June 2021
Available online 29 June 2021

rolling elements, which leads to both axial and radial vibrations [1]. Manufacturing inaccuracy induced waviness occurring in rolling elements or inner and outer bearing rings are known sources of vibration [1,2].

There are several experimental studies in literature that investigate the effect of bearing waviness, mainly for ball bearings. For example, Wardle [3] using measured waviness of the ball and raceway surface, obtained bearing excitation forces close to the values predicted in his theoretical model [4]. In other experimental studies, Liu et al. [5] measured the actual waviness, while Shah and Patel [6] and Babu et al. [7] generated artificial waviness on the surface of inner and outer rings and used these waviness values as excitation source. Such experimental studies have often investigated the effect of outer ring waviness [5,8], inner ring waviness [7] or a combination of both [9].

Researchers have proposed many different methods for including the effect of waviness in bearing models. In a broader classification based on solution methods, rotor dynamic systems that include multiple sources of excitation, such as unbalance, asymmetry, bearing waviness and other bearing related defects, are mostly solved using either time domain or frequency domain based analysis. In time domain analysis, the general approach is to numerically solve the system equations using a time integration scheme. In the frequency domain approach, on the other hand, the harmonic forced response is directly obtained by solving the analytical equation of motion for the excitation source [10].

A large number of papers in the literature use the time domain approach to correlate the amplitude and wavelength of bearing waviness with excitation forces, frequencies and overall system response [4]. Harsha et al. [11] utilized the Hertzian contact theory to calculate the elastic deflection and nonlinear contact force. They investigated the effects of waviness in the inner and outer rings with assumed values of waviness amplitude and phase. Cao and Xiao [12] also included surface imperfections of balls or rollers in their models in the form of sinusoidal functions. Using the time domain approach, many researchers have considered the effect of waviness in their models for different types of bearings, for example, deep groove ball bearings [13–16], angular contact ball bearing [17], aeroelastic journal bearings [18] and cylindrical roller bearings [19,20]. Zhang et al. [21,22] investigated the effect of multiple excitations such as unbalance, waviness and bearing preload on instability of the rotor and found that waviness amplitude has the greatest effect in the instability regions. Sopanen and Mikkola [13,14] considered the combined effect of waviness along with bearing clearance and localized defect.

In general, time domain based studies have tended to use numeric integration tools such as the Runge–Kutta method [23] and Runge–Kutta-Fehlberg algorithm [24] or a combination of implicit methods such as the Newmark-β with the Newton–Raphson method to iteratively solve the nonlinear differential equations, as can be seen in the studies by Harsha and Kankar [25] and Harsha et al. [11,26].

In an experimental study investigating spherical roller bearings, Viitala et al. [27] efficiently reduced the subcritical vibrations by modifying the bearing roundness profile in a large tubular rotor case. Heikkinen et al. [28] proposed a time domain based numerical integration method to simulate the effect of bearing waviness in rotor systems studied in [27]. The simulated model emphasized the significant effect of half critical subharmonic vibrations. Kurvinen et al. [29] further expanded the study by including the effects of the third and fourth waviness components.

Almost all studies using available bearing modelling methods have solved the system equations in the time domain and then analyzed the response in the frequency domain. This is because the time domain signal does not provide information about the frequency or amplitude of the unfiltered signal needed for system analysis, especially if the signal is recorded for a short period [30].

One crucial limitation when solving a nonlinear dynamic model in a time-based iterative method is the computational time [18]. Depending on the parameters of the simulation, the level of detail in the model, and the time step, the computational burden might be quite large [31].

An alternative approach to solving a nonlinear dynamic model in a time-based iterative method and analyzing it in the frequency domain is to solve the rotor-bearing model in the frequency domain itself. While Saito [32] has utilized frequency based methods such as harmonic balance to investigate the effect of radial clearance in bearings for an unbalanced Jeffcott rotor, as per the authors knowledge, there is little research on solving dynamic rotor models that include bearing waviness in the frequency domain. Thus far, only one research paper has demonstrated use of the frequency domain approach for solving responses caused by bearing waviness, namely, Ono and Okada [33], who studied vibrations caused by outer ring waviness for a single degree-of-freedom (DOF) model of an automobile drive shaft. Therefore, it would appear that although frequency domain analysis of the vibration signal is a conventional approach for bearing diagnosis in purely experimental studies and in industry, frequency domain solution methods are not commonly used when modeling bearing behavior, where most models are solved in the time domain and the results are then converted and interpreted in the frequency domain. However, this approach is not computationally efficient, hindering its use in, e.g., design space explorations, genetic algorithms for optimization and parameter estimation, which are all problems of iterative nature. Computational efficiency is also desired in Digital Twins [34], which may include machine learning and real-time characteristics.

This paper aims to contribute to the field by bridging the research gaps related to:

(1) the computational efficiency of the rotor-bearing systems simulations considering the bearing waviness as an excitation source,
(2) the frequency domain solution for the simulation of the bearing waviness,
(3) the lack of experimental verification for bearing waviness frequency domain solutions.

The current study proposes two novel methods for solving the responses caused by bearing waviness excitation in the frequency domain. In the study, waviness is considered as a base motion that transmits multiple harmonic excitation forces to the rotor through bearing stiffness and damping. The methods proposed are:

(1) Base Excitation Method (BEM): Here, the excitation forces for each harmonic component are calculated as spring and damping forces, using the waviness components directly as the excitation source. Once the displacements for each harmonic excitation are solved, they are combined using the principle of superposition [10].
(2) The Bearing Kinematics Augmented Base Excitation Method (BKA-BEM): The base excitation method is augmented with the bearing kinematics by calculating the relative rotor displacement from a 4-DOF nonlinear quasi-static bearing model that accounts for bearing waviness and clearance. The displacements obtained for one revolution of the bearing model are split into its harmonic components using Fast Fourier Transform (FFT). These refined displacements are used as the excitation source in the forced displacement equation instead of direct waviness. The solved response for each harmonic component is superpositioned using the same principle as the Base Excitation Method.

The present study verifies both frequency domain-based solution methods using a case study of a paper machine roll mounted on spherical roller bearings. The measured inner ring waviness is used as input for the excitation source and the vibration amplitude at subcritical harmonic resonances are obtained at the middle of the rotor. The results obtained from each solution method are compared to those obtained from a previously designed time domain-based solution method [28,29] for numerical validation. The responses are also compared with measured responses for experimental verification.

2. Modelling methods

2.1. Rotordynamic modelling methods

For modeling rotating machines, finite element methods (FEM) are widely used. Here, the rotor is discretized using nodes and elements, and other components, such as bearings and supports, are integrated in the nodes corresponding to their actual locations [35].

To solve nonlinear or linear systems under harmonic or non–harmonic excitation, the numerical time integration approach can be used to calculate the transient response for variable speed and a given time interval [36]. Alternatively, in the linearized frequency domain approach, a receptance matrix and the components of the harmonic forces are used to solve the coefficient vectors for the assumed harmonic solution, therefore generating steady state response as a function of frequency [37].

2.2. General bearing modelling method with inner ring waviness

In general, rolling elements of a bearing act as an intermediate structure between a rotor and its supports. The inner and outer rings of the bearing are rigidly fixed to the rotor and the support respectively. For increased computational efficiency, some simplifications in the bearing model are carried out as follows:

(1) There is no slipping or sliding between the bearing components, and all balls or rollers move around the raceways at an equal velocity.
(2) There is no bending deformation of the raceways.
(3) Centrifugal forces acting on the rolling elements are neglected.
(4) Contact between the rolling elements and the rings is linearized at equilibrium condition with given load. The linearized forces also account for radial clearance.

The proposed solution methods for solving responses caused by bearing waviness in the frequency domain are applicable to all bearing models that define the contact between the races and the rolling elements as non-linear springs and where the deformations are modelled using non-linear force displacement relations. Thus the methods can be used with typical rolling element bearings, such as a deep groove ball bearings (DGBB) [13,14], high speed angular contact ball bearings (ACBB) [38] and spherical roller bearing (SRB) [39]. For the purpose of completeness and to elaborate the method, the general rolling element bearing (REB) equations used to formulate the kinematics and model are briefly described.

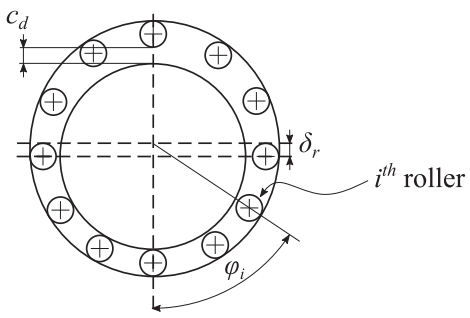

Fig. 1. Generalized rolling element bearing.

Fig. 1 illustrates a generalized, single row REB where the effect of bearing clearance is included [1].
Elastic deformation of the ith rolling element in the direction of load can be given as:

$$\delta_i = \delta_r \cos(\varphi_i) - c_d/2 \tag{1}$$

where δ_r is the radial displacement and φ_i is the attitude angle of the ith rolling element. The effect of inner ring waviness of a bearing can be added in the elastic deformation equation as:

$$\delta_i^w = \delta_i + \sum_{k=1}^{n} A_k \cos[k(\varphi_i - \theta) + \phi_k] \tag{2}$$

where d_i^w is the elastic deformation due to the bearing inner ring waviness, θ is the rotation angle of the inner ring, k the harmonic waviness order, A_k and ϕ_k are the kth order waviness amplitude and phase angle, respectively.

Using the total elastic deformation from Eq. (2) and Hertzian contact theory, the contact force of each rolling element having positive contact deformation is given as:

$$F_j^i = k_c^{tot} \left(\delta_i^w\right)^n \tag{3}$$

where n is 1.5 for DGBB, ACBB and SRB and 1.08 for a cylindrical roller bearing, k_c^{tot} is the total contact stiffness coefficient of the rolling element, considering both inner and outer ring contact areas. The total bearing forces in different translational directions can be calculated as a sum of forces from all individual rolling elements. At equilibrium condition, the linearized bearing stiffness coefficients can be obtained by the partial derivative of the bearing loads with respect to the displacements of the bearing [22].

For systems operating at low and medium rotation speeds the centrifugal forces generated in the roller elements do not have significant effect to the bearing stiffness and therefore an assumption of constant bearing stiffness model can be used. However, for high speed machines, the centrifugal forces are significant and therefore, the bearings properties are speed dependent [40]. In such a case bearing model as proposed in [38] can be used where the centrifugal forces are accounted for and the bearing stiffness is calculated at each speed.

2.3. Principle of superposition and the Base Excitation Method (BEM)

In this method, the waviness is assumed to directly affect the rotor and support movement. Therefore, instead of using a detailed bearing modeling method, the excitation is assumed to cause forced displacement between the inner ring (rotor) and the outer ring (support). Fig. 2 shows the model where the inner ring waviness acts as a base excitation. The waviness excitation is applied to two points, in the vertical and horizontal directions, respectively. The followers are fixed and based on the position of the rotor, the excitation at the corresponding point is transferred to the rotor via the bearing as forced excitation. Both the bearing and support are modelled as spring damper elements in series. The excitations from the vertical (ver) and horizontal (hor) directions are independent with no cross-coupling between them.

In general, bearing waviness is considered as a combination of sinusoidal imperfections on the surface of the ring in the shape of peaks and valleys. Based on the order of these imperfections, waviness generates several harmonic excitations [41]. Displacement due to the kth harmonic waviness excitation can be written as:

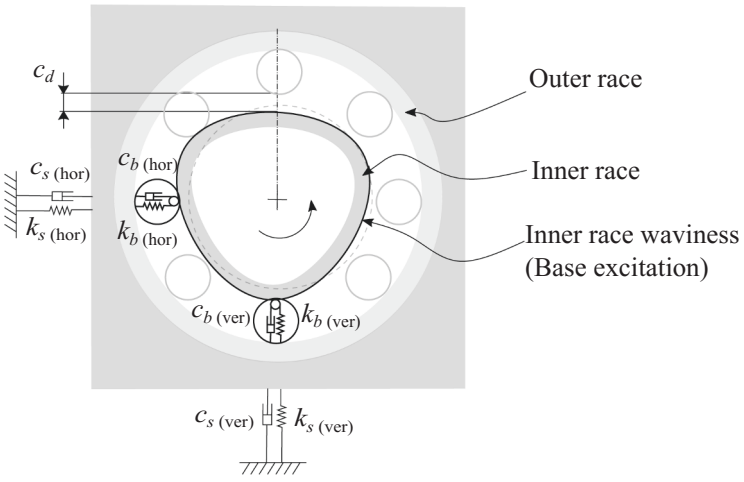

Fig. 2. Base excitation method (BEM) where the inner ring waviness is considered as a base excitation that is transferred to the rotor at two points, vertically and horizontally, independently.

$$\delta_k = A_k \cos(k\omega t - \varphi_k) \tag{4}$$

where ω is the rotating frequency of the rotor. Waviness can be considered as a base motion, in which the excitation forces are transferred through the bearing stiffness and damping. Therefore, the combined harmonic spring and damping forces for the kth order waviness excitation acting on the rotor are:

$$F_b(t) = \underbrace{(-k_b A_k sin\phi_k - c_b A_k k\omega\, cos\phi_k)}_{\mathbf{F}_s^k} \sin k\omega t + \underbrace{(k_b A_k \cos\phi_k - c_b A_k k\omega \sin\phi_k)}_{\mathbf{F}_c^k} \cos k\omega t \tag{5}$$

Simultaneously, a counteracting force acts on the support with equal magnitude and opposite direction to F_b. Considering multiple waviness excitations, the equation of motion for any general rotor bearing system can be written as:

$$\mathbf{M}\ddot{\mathbf{x}}\left(t\right) + \left(\mathbf{C} + \omega\mathbf{G}\right)\dot{\mathbf{x}}\left(t\right) + \mathbf{K}\mathbf{x}\left(t\right) = \sum_k \left(\mathbf{F}_s^k \sin k\omega t + \mathbf{F}_c^k \cos k\omega t\right) + \mathbf{F}_{ub} + \mathbf{F}_g \tag{6}$$

where $\mathbf{M}, \mathbf{C}, \mathbf{G}$ and $\mathbf{K}$ are the mass, damping, gyroscopic and stiffness matrices of the rotating system, $\mathbf{F}_s^k$ and $\mathbf{F}_c^k$ are the bearing forces, and $\mathbf{F}_{ub}$ and $\mathbf{F}_g$ are the forces due to unbalance and gravity, respectively. These matrices are obtained from the finite element model of the rotor bearing system. The stiffness matrix $\mathbf{K}$ includes the stiffness of the rotor and the bearing coefficients at respective node location. Similarly, the damping matrix $\mathbf{C}$ includes non-rotating internal damping of the rotor and the bearing damping coefficients. The unbalance force $\mathbf{F}_{ub}$ can be written in its component form as:

$$\mathbf{F}_{ub} = \mathbf{F}_{s(ub)} \sin\omega t + \mathbf{F}_{c(ub)} \cos\omega t \tag{7}$$

$\mathbf{F}_g$ is the global gravity force vector which can be assembled from the elemental gravity force vectors that can be written for element i as follows:

$$\mathbf{F}_g^i = \rho A g \left[\frac{1}{2}L \quad 0 \quad 0 \quad \tfrac{1}{12}L \quad \tfrac{1}{2}L \quad 0 \quad 0 \quad -\tfrac{1}{12}L^2\right]^T \tag{8}$$

where ρ, A and L are the material density, cross-section area and length of the element, respectively. Acceleration of gravity, g, is applied in negative vertical direction. Note that while the external forces can be included in a more general analysis, $\mathbf{F}_g$ is constant and $\mathbf{F}_{ub}$ occurs once per revolution and therefore, their effects are not of interest in this study which focuses on subharmonic response. The terms $\ddot{\mathbf{x}}(t), \dot{\mathbf{x}}(t), \mathbf{x}(t)$ in Eq. (6) represent the acceleration, velocity and displacement vectors respectively. The solution of each individual harmonic excitation from Eq. (6) can be combined using the principle of superposition as follows:

$$\mathbf{x}\left(t\right) = \sum_k \left(\mathbf{a}^k \sin k\omega t + \mathbf{b}^k \cos k\omega t\right) \tag{9}$$

where the coefficient vectors $\mathbf{a}^k$ and $\mathbf{b}^k$ for each kth harmonic excitation are obtained as:

$$\begin{bmatrix}\mathbf{a}^k \\ \mathbf{b}^k\end{bmatrix} = \begin{bmatrix}\mathbf{K} - (k\omega)^2\mathbf{M} & -(k\omega)(\mathbf{C} + \omega\mathbf{G}) \\ (k\omega)(\mathbf{C} + \omega\mathbf{G}) & \mathbf{K} - (k\omega)^2\mathbf{M}\end{bmatrix}^{-1} \begin{bmatrix}\mathbf{F}_s^k \\ \mathbf{F}_c^k\end{bmatrix} \tag{10}$$

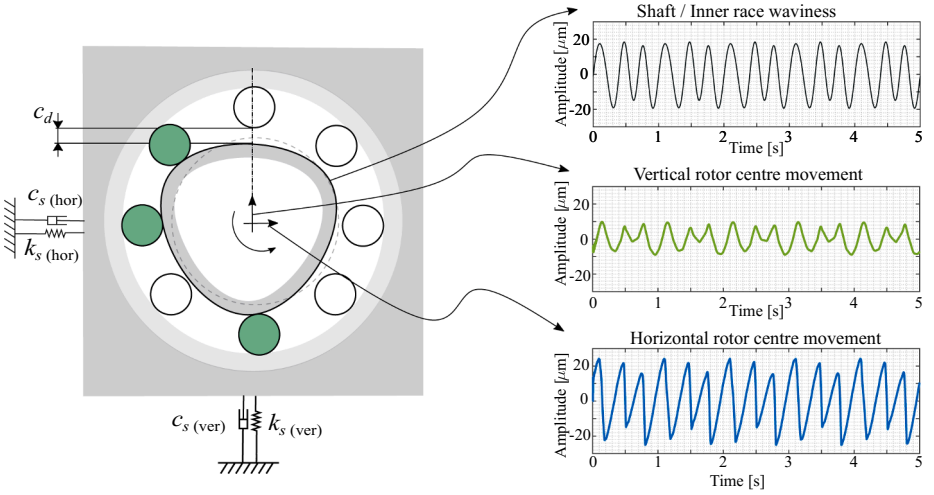

Fig. 3. 4-DOF roller element model where bearing kinematics is included in the response calculations.

2.4. Bearing Kinematics Augmented Base Excitation Method (BKA-BEM)

In the second method, the input waviness amplitudes are refined with the bearing kinematics. For that purpose, a 4-DOF quasi-static model is proposed that includes the effect of bearing clearance and waviness. It should be noted that other modelling approaches could be used for this purpose, e.g. a purely kinematic model. However, the proposed model takes into account the internal contact deformation of the bearing due to static loading while neglecting interconnected rotor-bearing dynamics.

In Fig. 3, the plot on top right shows the inner ring waviness used as input in the 4-DOF, bearing kinematics augmented base excitation method (BKA-BEM). Compared to the simple BEM proposed in Section 2.3 where the excitation was transmitted for two independent points only, in this method the excitation is transferred through all the rolling elements that are in contact with the inner ring waviness (rolling elements in contact at the time instant are shown in green in Fig. 3). The equation of motion for the 4-DOF bearing model is transformed into a first order ODE and solved using time integration. As the complexities of the rotor-bearing dynamics are not included and the number of DOFs in the calculation are significantly reduced, the process is computationally efficient. As an example, the plots on the right of Fig. 3 compare the input excitation of low order waviness with the vertical and horizontal response of the rotor. The output response includes the effect of the different harmonic components of the inner race waviness and as visible from the second and third plots in Fig. 3, the vertical and horizontal movement of the center point of the rotor are a combination of the bearing waviness, clearance and bearing deformation under static load.

In the next step, using Fast Fourier Transform (FFT), the individual harmonic amplitudes and phase are obtained both for the vertical and the horizontal components, which are then transferred into Eq. (5) to obtain the individual harmonic forces.

3. Case study and simulation models

To validate the proposed methods, a case study of an industrial scale spherical roller bearing (SRB) supported paper machine roll is used. The measured inner ring waviness of the bearings is used as input in the simulation models and the response is obtained at the middle of the rotor. The numerical results calculated by the proposed frequency domain solution methods are compared with:

(1) Numerical results of a high-fidelity model based on a time domain solution method (TDSM) that was developed by Ghalamchi et al. [39] and validated in previous studies [28,29].
(2) Measured response at the middle of the roll supported by the spherical roller bearing as reported by Viitala et al. [27]

3.1. Test rig and measurement setup for experimental validation

A guide roll on a paper machine, i.e. a large cylindrical roll-type rotor made of steel, was selected for the test case. The mass of the roll is 720 kg, the tubular section is 4 m long and the end shafts total 1 m. The roll is supported with a SKF 23124 CCK/W33 bearing with a conical adapter sleeve H 3124. The bearings are connected to support structures that have high vertical stiffness and considerable flexibility in the horizontal direction. The asymmetry in the support separates the natural frequencies of the first bending modes well, being 21 Hz in the horizontal and 30 Hz in the vertical directions, respectively. The supports at the two ends are entirely separate, and they thus do not include significant cross-coupling effects.

The measurement procedure and setup has been described extensively in previous studies [27,29] and are included herein in a concise manner for the sake of completeness. Fig. 4 shows the experimental rotor and setup.

The roundness profile of the inner ring of the bearing was measured during installation of the rotor shaft. This measurement ensured that the acquired roundness profile was the actual roundness profile of the inner ring in operating conditions. The roundness profile was measured utilizing a four-point method [42]. The bearing was disassembled to enable modification of the bearing geometry. The roundness profile of the installed bearing inner ring was modified by inserting thin steel shims between the rotor shaft and

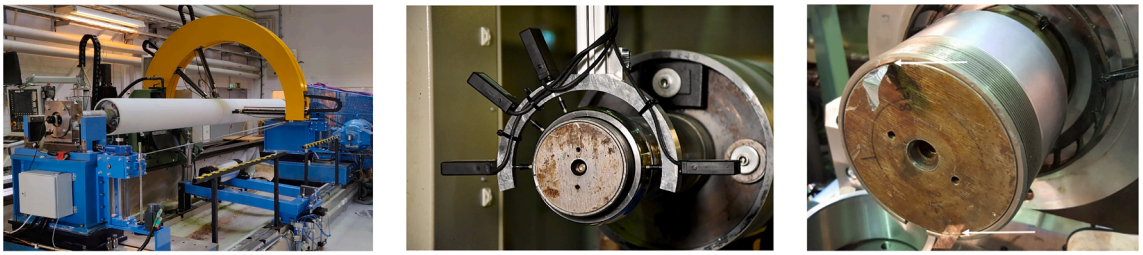

(a) (b) (c)

Fig. 4. Experimental test rotor: (a) Measurement setup; (b) The roundness profile measurement of the bearing inner ring during installation of the rotor shaft; (c) The roundness profile of the inner ring of the bearing was modified by inserting steel shims between the conical adapter sleeve and the rotor shaft. [27].

the conical bearing adapter sleeve. Three different roundness profiles of the inner ring of the bearing were measured at the service end of the rotor: original, oval and triangular. The drive end was not modified, but the roundness profile was measured nevertheless.

The study of different profiles was carried out to observe how the geometry of the excitation source directly correlates to the amplitudes of the corresponding response peaks. Moreover, it also enabled the verification of the proposed methods by testing their ability to simulate the amplitudes close to the measured peaks for different roundness profiles. The experimental rotor system and the measurement results are presented by Viitala et al. [27]. The dynamic response of the rotor was measured utilizing a measurement environment built on a commercial roll grinding machine. The measured response was obtained in the horizontal and vertical directions at the middle cross-section of the rotor at a rotational frequency range of 4–18 Hz with 0.05 Hz increments using the four-point method to extract the roundness profile and the rotor center point movement from the measured signals of four laser sensors. An encoder was used to collect 1024 samples per revolution. Data sets containing a hundred revolutions were acquired at each rotational frequency step. The data sets were synchronously averaged [43] to reduce noise and measurement uncertainty. Finally, the center point movement data was analyzed using FFT to obtain the response spectra of the rotor in the horizontal and vertical directions.

The measured inner ring waviness used in the models is shown in Table 1. As the table shows, the amplitude of the 2nd and 3rd components is higher in case 2 and case 3, respectively, as the roundness profiles have been manipulated to oval and triangular shapes using steel shims in the test rig. These changes were made in the SRB at the service side while the drive side bearing roundness profile remained the same.

3.2. Rotor model description

The rotor is modelled using Timoshenko beam element [44] with two translational and two rotational degrees of freedom (DOF) at each node (Fig. 5). The bearing models developed in this study are connected to the nodes that represent their respective location in the actual test rig. In Fig. 5, for simplicity, k_{eq} and c_{eq} represent the bearing coefficients in combination with highly anisotropic support structures which have considerably higher stiffness in vertical direction than in the horizontal direction. As there is almost no cross-coupling between supports in this test rotor, a concentrated parameter approach is utilized by simplifying the support into horizontal and vertical spring-mass-damper elements [45]. The corresponding support stiffness values in the horizontal and vertical directions are 18 MN/m and 200 MN/m, respectively. The rotor model is validated with free-free frequencies and supported frequencies measured from the actual machine, i.e. 75 Hz for the free-free rotor, and supported frequencies of 20.9 Hz in the horizontal direction and 30 Hz in the vertical direction.

3.3. Description of the bearing model

The industrial-scale bearing used in the test case is modelled using a SRB model originally developed by Ghalamchi et al. [39].

Table 1
Bearing waviness amplitudes and phases used in the simulation models.

		First roller element path		Second roller element path	
	k	Amplitude (A_k) [μm]	Phase (ϕ_k) [deg]	Amplitude (A_k) [μm]	Phase (ϕ_k) [deg]
Service end		Case 1 – original			
	1	0	0	0	0
	2	10.03	319.3	7.16	320.7
	3	2.61	80.8	3.06	75.7
	4	4.23	63.7	4.69	69.0
		Case 2 – oval			
	1	0	0	0	0
	2	18.14	284.3	16.32	284.1
	3	2.29	86.2	3.09	71.4
	4	9.83	359.8	8.49	353.3
		Case 3 – triangular			
	1	0	0	0	0
	2	7.32	282.9	6.22	293.7
	3	16.45	58.7	15.92	57.9
	4	4.82	9.7	4.93	3.5
Drive end	1	0	0	0	0
	2	2.95	265.5	2.65	279.4
	3	1.06	228.1	0.43	182.5
	4	0.67	190.2	0.91	265.5

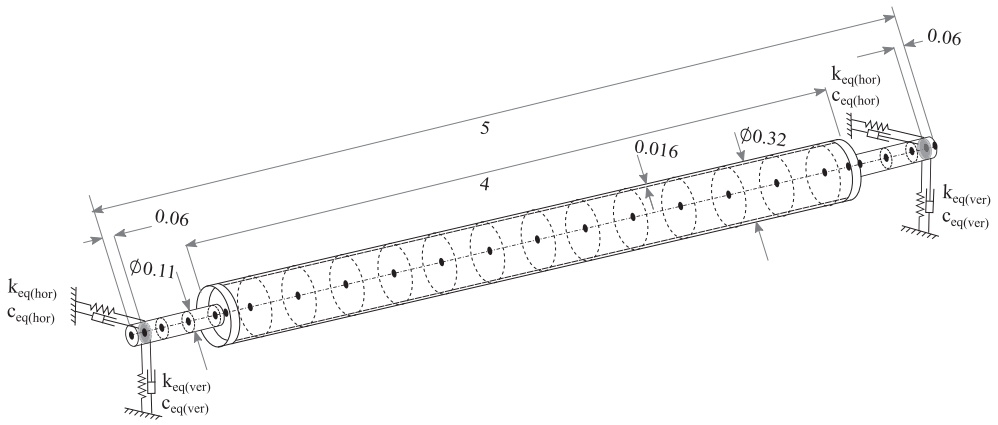

Fig. 5. Wireframe sketch of the guide roll of a paper machine (test rotor) with FE discretization. All dimensions are in meters.

Details of the model, including the bearing dimensions, modelling parameters and force equations can be found in [29]. In this study, the model is developed further to obtain linearized bearing stiffness coefficients. Therefore, to keep the material concise and to avoid repetition, only additional development of the bearing model is discussed in the following subsections.

3.3.1. *Bearing equilibrium and linearized bearing stiffness coefficients*

The stiffness of the SRB model can be obtained by solving the bearing equilibrium and the force displacement relation using the Newton–Raphson method. Bearing equilibrium occurs when the internal forces at the bearing are equal to the external load acting on the bearing. The external load, $\mathbf{F}_r$, acting on the bearing comes from the static loading that the bearings experience when used. Using initial values for displacement and velocity, the internal bearing forces ($\mathbf{F}_b$) can be calculated from the bearing model in Section 2.

For a small perturbation of Δ_h, the residual force at that step and the equation for iteration by Newton–Raphson method can be represented as:

$$\mathbf{F}_{res}^{(h)} = \mathbf{F}_b - \mathbf{F}_r \tag{11}$$

$$\delta^{(h+1)} = \delta^{(h)} - (\mathbf{F}(\Delta_\mathrm{h})/\Delta_\mathrm{h})^{-1} \cdot \mathbf{F}_{res}^{(h)} \tag{12}$$

The equilibrium condition is achieved using a predefined convergence criterion ($1e^{-10} \cdot \mathrm{norm}(\mathbf{F}_{res}^{(h)})$). At this equilibrium state, the linearized stiffness of the bearing can be obtained as:

$$\mathbf{K}_b = (\mathbf{F}(\Delta_\mathrm{h})/\Delta_\mathrm{h}) \tag{13}$$

The linearized bearing stiffness coefficients obtained using the above formulation for the SRB bearings in the test case are as shown in Table 2.

Table 2 shows that the linearized stiffness is notably higher in the vertical direction compared to the horizontal. It is known from Krämer [41] that the lateral stiffness is smaller than the in-line stiffness. However, the excessive difference in stiffness probably occurs because the applied load (about 3.5 kN) is very low compared to the nominal dynamic load capacity of the SKF 23124 CCK/W33 bearing (534 kN). Note that fixed bearing coefficients are used in the simulation models of the test case. This is because in the low to moderate speed range in the studied system, the bearing stiffness do not change as a function of speed [46].

3.3.2. *Vectorial averaging of waviness components for BEM*

The general BEM is directly applicable to bearings with single row rolling elements. Since the SRB model in the test case has two roller rows, a vectorial average is calculated to find the resultant waviness amplitude and phase for each excitation component. The waviness component from each row is divided into their horizontal and vertical vectors. These vectors are then added, combined into a resultant vector and averaged (divided by 2 since there are two rows) to obtain a single resultant amplitude and phase for the BEM.

3.3.3. *Procedure for bearing kinematic augmentation in BKA-BEM and results post-processing*

The base excitation method is augmented with the bearing kinematics, as proposed in method 2, using a 4-DOF bearing model. The

Table 2
Linearized stiffness values in the vertical and horizontal direction.

Direction	Stiffness coefficient (N/m)
Vertical	$1.0642 \cdot 10^9$
Horizontal	$1.0145 \cdot 10^8$

bearing model takes the measured inner ring waviness as the input for excitation and uses a numerical time integration scheme to determine the system response. However, for simplification and fast calculation, the rotor is simplified into two equally divided lumped masses (720/2 = 360 kg), one for each bearing. The bearing model is solved for one bearing at a time. Since each bearing has two rows of rollers, two different waviness signals are built using Eq. (2) and measured amplitudes and phase values from Table 1. The waviness signals are used as the input excitation in the 4-DOF quasi-static model and the model yields the relative displacements between the rotor and the support in the horizontal and vertical directions as the output. As an example, Fig. 6 shows the input and the output signal for the original roundness profile (Case 1) of the test case.

Fig. 6 also shows the post processing step for the output displacements (both horizontal and vertical) obtained from the model. The amplitudes and phases for the fist four harmonics (from 1st to 4th component) are obtained using Fast Fourier Transform (FFT) for each of the response signal. Higher order harmonics are neglected as the FFT shows a significant drop in amplitude after the 4th component and because, for this particular test case, the study focuses on low order waviness components. The same process is applied to the other cases with different roundness profile (original, oval and triangular) at the service end as well as for the drive end bearing with a fixed roundness profile. Fig. 7 shows a comparison between the input waviness component and the output from the model augmented with the bearing kinematics. The amplitudes of the output response are summarized in Table 3. These amplitudes and

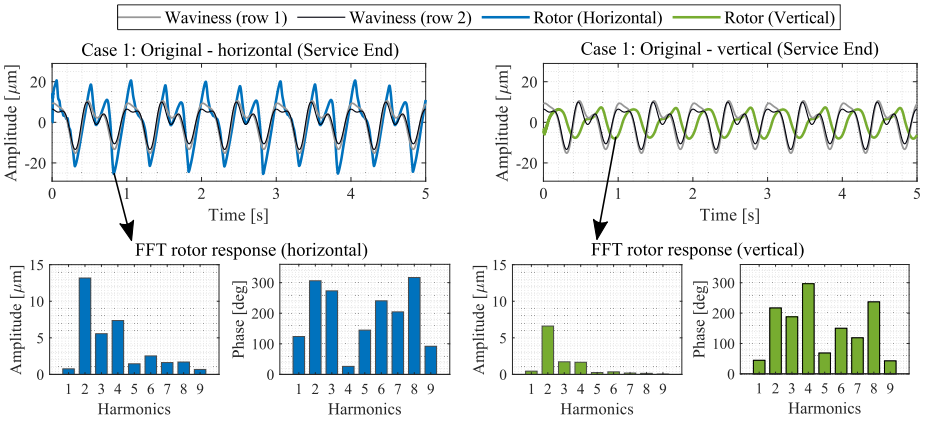

Fig. 6. Waviness profile (input) and relative rotor displacement (output) from the 4-DOF quasi-static bearing model in the horizontal (left) and vertical (right) direction for the original inner ring profile (Case 1).

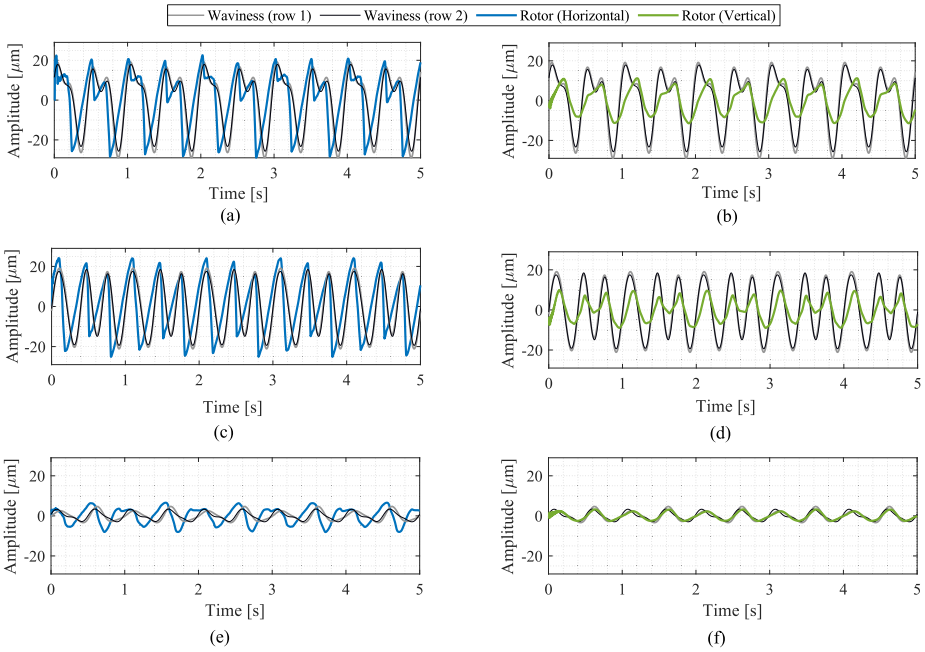

Fig. 7. Waviness profile (input) and relative rotor displacement (output) from the 4-DOF bearing kinematic model in the horizontal (left) and vertical (right) direction for the service end ((a), (b), (c), (d)) and drive end ((e), (f)) bearings. In the service end, (a) and (b) are for Case 2 (oval) while (c) and (d) are for Case 3 (triangular) roundness profile. (e) and (f) are for the unchanged original roundness profile in the drive end.

Table 3
Amplitude and phase values obtained from FFT of the BKA-BEM output for different waviness profile at the service end and fixed profile at drive end.

		Vertical		Horizontal	
	k	Amplitude (A_k) [μm]	Phase (ϕ_k) [deg]	Amplitude (A_k) [μm]	Phase (ϕ_k) [deg]
Service end			Case 1 – original		
	1	0.45	44.5	0.76	123.8
	2	6.61	216.8	13.18	306.3
	3	1.72	187.8	5.57	273.3
	4	1.66	296.8	7.36	26.3
			Case 2 – oval		
	1	1.45	228.4	0.76	304.4
	2	9.03	244.2	13.18	329.8
	3	1.09	205.4	5.57	286.8
	4	1.69	15.2	7.36	99.3
			Case 3 – triangular		
	1	1.25	152.3	1.13	230.8
	2	4.13	245.5	7.64	335.8
	3	5.93	211.0	16.48	297.7
	4	0.77	352.3	2.46	78.0
Drive end	1	0.03	102.4	0.06	179.6
	2	2.49	267.1	5.24	356.4
	3	0.49	54.2	1.67	141.8
	4	0.31	125.5	1.63	213.3

phases are then plugged into the Base Excitation Model (Eq. (5)) of the rotor bearing system for both bearings and the overall rotor response is obtained through Eqs. (6)–(10).

3.4. High-fidelity model used for numerical validation

The high-fidelity model uses a TDSM-based nonlinear spherical roller bearing model combined with an asymmetric model of the rotor. The model has been developed previously and validated in several studies [28,29]. In this study, the TDSM model is used as a numerical benchmark for the two proposed methods.

The spherical roller bearing model, originally developed by Ghalamchi et al. [39], uses Hertzian contact theory to calculate the nonlinear contact force for each roller. The nominal bearing clearance used in this model is 60 μm and inner ring waviness components of twice to four times per revolution are used from Table 1. The SRB model is combined with an FE-model of the flexible rotor. The asymmetry of the rotor shaft is accounted for in this model by including the thickness variation of the hollow tube section of the rotor along its length based on ultrasonic measurement [28,47]. Similar to the other models, the supports are modelled here as mass-spring-damper elements individually in the horizontal and vertical directions.

Time integration is used to solve the nonlinear bearing model and the asymmetric rotor model. For the numerical solution, model reduction is applied using the assumed-modes method [48], and the model is solved with 16 retained modes. Simulation runs are conducted for 9 s with a sampling rate of 2000 Hz (time-step of 0.0005 s).

4. Results

In this section, the responses obtained with the proposed frequency domain-based methods, i.e. BEM and BKA-BEM, are compared with the numerical output of the time domain solution method (TDSM) and the measured response. The responses are measured at the center of the rotor and the responses are extracted from the same node location in each method. Since the test rotor operates in the subcritical frequency range, the subcritical resonance peaks occurring at fractions of the critical frequency are of key interest. All simulations were conducted for frequency range similar to the measured rational speed range, i.e. 4–18 Hz. For each case, the horizontal and vertical amplitudes are compared separately, and a bar chart is used to compare the peak values.

4.1. Case 1: Original bearing waviness profile

In Case 1, the inherent waviness profile is used without any modifications. With this input waviness profile (Table 1), the 2nd component has the highest amplitude, which is reflected in the response in Fig. 8. In both the horizontal and vertical direction, the 2nd

component contributes to the highest vibration followed by the 3rd and 4th subcritical components.

The proposed BKA-BEM and BEM based models are able to follow closely the measured peak frequencies, both in the vertical and the horizontal direction. Furthermore, the BKA-BEM model can generate responses with almost similar accuracy to the high-fidelity TDSM model. The BEM model is able to provide accurate estimation of the frequencies. However, compared to the other methods, it is unable to generate the response amplitudes accurately as it undershoots in the horizontal direction while overshooting in the vertical direction. Especially at the 4th subcritical harmonic peak in the vertical direction, the BEM model behaves irregularly with a high response amplitude (about 10 times higher than the measured response).

4.2. Case 2: Oval bearing waviness profile

In Case 2, the inner ring waviness profile in the service end is modified to an oval shape using thin steel shims. Fig. 9(a,b) show the response in the horizontal and vertical direction respectively with the oval waviness profile as input excitation. As expected, due to the oval shape the twice-per-rotation component or the 2nd subcritical harmonic shows the highest response while the 3rd and 4th subcritical harmonic responses are comparatively lower. Compared to the original case (Case 1), the 2nd component shows a significant increase in the response due to the increase in ovality of the inner ring waviness profile.

In the horizontal direction, both the BKA-BEM model and the BEM based model follow the reference measured response and the TDSM based model very closely, with the BEM model almost directly overlapping the measured 2nd harmonic peak. In the vertical direction, the 2nd harmonic peak in the measured response is about 238 μm, closely followed by the BEM model at 194 μm. The amplitude from the TDSM and BKA-BEM peaks for the 2nd harmonic component are in the 350–500 μm range. Similar to Case 1, the BEM model follows the measured response very well at all the peaks, except for the 4th subcritical harmonic peak where it shows the same amplifying behavior of a very high response amplitude (about 34 times higher than the measured response).

4.3. Case 3: Triangular bearing waviness profile

In Case 3, the inner ring waviness profile in the service end is modified into a triangular geometry, meaning the 3rd harmonic component has the largest amplitude and makes a major contribution to the overall response. Fig. 10 shows the response of the system where unlike the previous cases, the amplitude of the third subcritical harmonic peak has significantly increased. Fig. 10(a) shows that the horizontal 2nd, 3rd and 4th subcritical harmonic peaks for all three models deviate by 0.5–1 Hz from the measured frequencies for the respective peaks. The amplitudes in the horizontal peaks for the BKA-BEM and TDSM model are close to the measured amplitudes, especially for the 3rd harmonic peak.

In the vertical direction, the BEM again follows the measured response very well, particularly at the 3rd subcritical harmonic peak. The BKA-BEM model, although following the TDSM model quite closely, shows lower amplitudes in the vertical direction. Unlike cases 1 and 2, the BEM model does not show a large surge in the 4th subcritical harmonic peak amplitude.

Table 4 shows the estimated natural frequencies in the horizontal and vertical direction for the anisotropic system. The frequencies are estimated using the rotating frequencies at which the sub harmonic resonance peaks occurred for each case (2nd sub harmonic resonance frequency is half the natural frequency, 3rd sub harmonic resonance frequency is one third of the natural frequency, etc.).

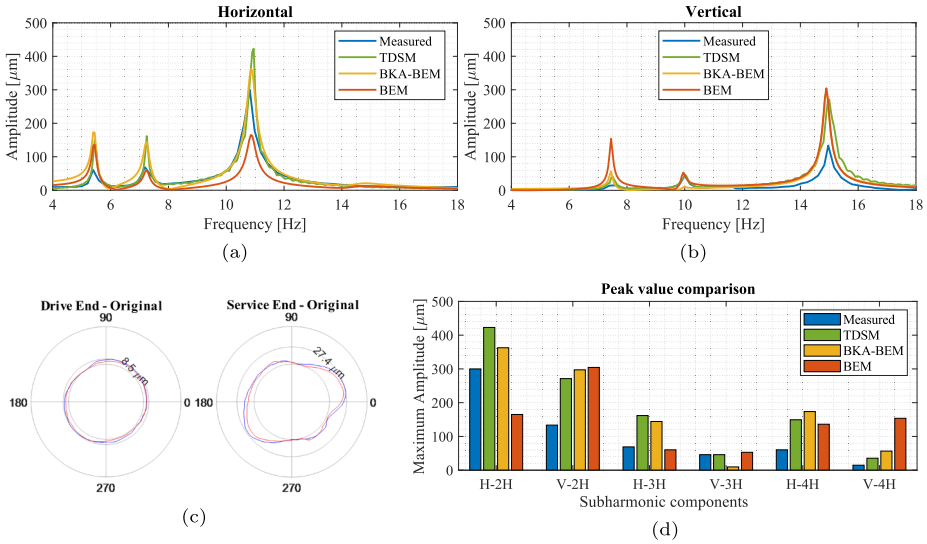

Fig. 8. Original Case (Case 1): Response obtained using the two proposed frequency domain solution methods (BKA-BEM and BEM) compared to the time domain solution method (TDSM) and the measured response in (a) the horizontal direction and (b) the vertical direction (c) Measured input waviness profile (two roller rows for each bearing) (d) Comparison of maximum amplitudes at sub-harmonic resonance peaks.

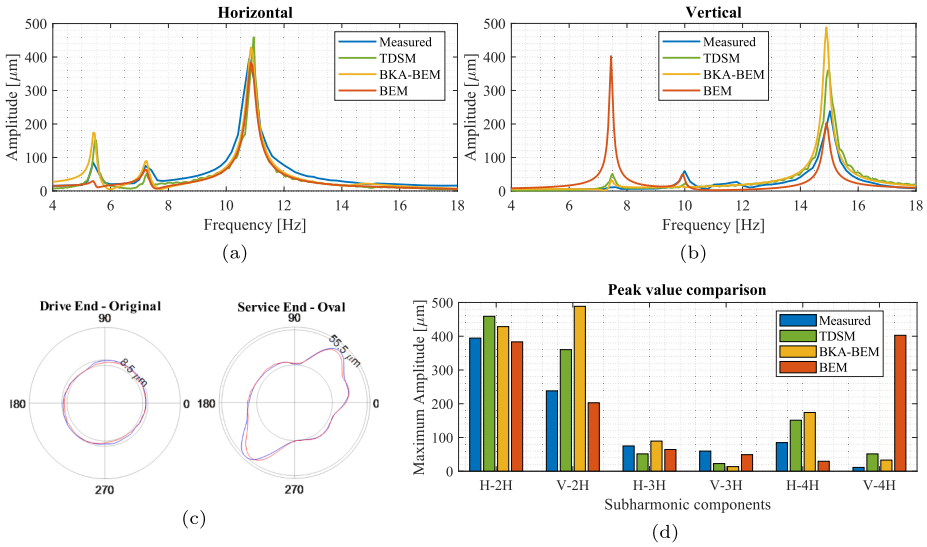

Fig. 9. Oval Case (Case 2): Response obtained using the two proposed frequency domain solution methods (BKA-BEM and BEM) compared with the time domain solution method (TDSM) and the measured response in: (a) Horizontal direction; (b) Vertical direction. (c) Measured input waviness profile (two rollers for each bearing) (d) Comparison of maximum amplitudes at sub-harmonic resonance peaks.

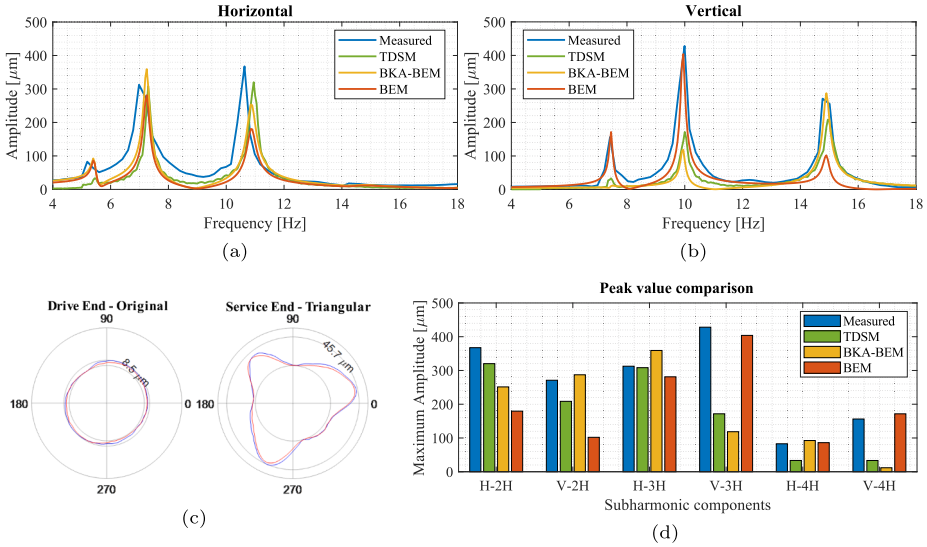

Fig. 10. Triangular Case (Case 3): Response obtained using the two proposed frequency domain solution methods (BKA-BEM and BEM) compared to the time domain solution method (TDSM) and the measured response in: (a) Horizontal direction, and (b) Vertical direction. (c) Measured input waviness profile (two rollers for each bearing). (d) Comparison of maximum amplitudes at sub-harmonic resonance peaks.

The natural frequencies calculated from each subcritical component is then averaged for each case and each model (highlighted in blue). In the measured response, the natural frequency in the vertical direction remains almost unchanged for the different inner ring roundness profiles. In the horizontal direction, the natural frequency increases by 0.7 Hz for the oval case, and then drops back to 21 Hz for the triangular case. The different models have more or less similar estimation for the natural frequencies; however, the slight variation in horizontal frequencies for the different roundness profiles in the measured results are not observable in the estimated frequencies from the models.

5. Discussion

In the results section, the displacement measured at the center of the rotor is compared with the response at the same location from three different models: BEM, BKA-BEM and a detailed, time domain-based model. The amplitudes of the subcritical harmonic peaks are captured quite well for all three cases of different inner ring roundness profile. In general, the horizontal responses in the simulation

Table 4
Comparison of the accuracy of the different models in estimation of natural frequencies in the horizontal and vertical direction for cases 1, 2 and 3. The natural frequencies are calculated by multiplying the rotating frequency, at which a subharmonic resonance peak was detected, with the corresponding harmonic component number. The averaged values for natural frequencies for different models for each case are highlighted in blue.

Cases	1. Original				2. Oval				3. Triangular			
Sub Harmonics	2H	3H	4H	1st critical (Avg.)	2H	3H	4H	1st critical (Avg.)	2H	3H	4H	1st critical (Avg.)
Horizontal natural frequency [Hz]												
Measured	10.40	7.00	5.20	**20.87**	10.79	7.20	5.39	**21.58**	10.63	6.98	5.19	**20.99**
TDSM	10.95	7.25	5.45	21.82	10.95	7.25	5.45	21.82	10.90	7.30	5.45	21.83
BKA-BEM	10.85	7.25	5.40	21.68	10.85	7.20	5.40	21.63	10.85	7.25	5.40	21.68
BEM	10.85	7.25	5.45	21.75	10.85	7.20	5.40	21.63	10.85	7.25	5.40	21.68
Vertical natural frequency [Hz]												
Measured	14.90	10.01	7.60	**30.08**	15.02	9.99	7.61	**30.15**	14.77	9.99	7.41	**29.72**
TDSM	15.00	10.00	7.45	29.93	14.95	10.00	7.50	29.97	14.95	10.00	7.45	29.90
BKA-BEM	14.90	9.95	7.45	29.82	14.90	9.85	7.45	29.72	14.90	9.95	7.50	29.78
BEM	14.90	9.95	7.45	29.82	14.90	9.95	7.45	29.82	14.90	9.95	7.45	29.82

models have higher response than in the vertical direction because of the relatively low support stiffness in the horizontal direction (18 MN/m horizontal and 200 MN/m vertical support stiffness). The same trend can be observed in the measured response, with the exception of Case 3, where for a triangular roundness profile, both horizontal and vertical directions had high responses.

Another interesting behavior in the response plots is the correlation between the response peaks at the 2nd and 4th subcritical harmonic frequency, especially in the BEM model. For Case 1 (original) and Case 2 (oval), where the 2nd waviness component has the highest amplitude in the service side, the response peak at the 4th subcritical harmonic frequency is remarkably high for the BEM model. This high value is probably because the high 2nd component in the service side combines with the drive side components (where the 2nd waviness component has the highest amplitude as well) resulting in a cross-coupling effect. Depending on the phase difference between the roundness profiles at the two end, at certain alignment, the 2nd component from each end can combine to cause an excitation 4 times per revolution, causing an additional surge to the already existing 4th subcritical peak at the center of the rotor. Since the BEM method uses the raw waviness amplitudes and phases as the source of excitation, the effect is more prominent with the BEM method, probably causing the unusually high 4th subcritical response peak for cases 1 and 2.

Assessment of the results can provide further insight into the performance of the models compared to measurement, especially for the two proposed models, BKA-BEM and BEM. The experimentally measured response is considered as a guide for performance evaluation, while the previously studied and verified TDSM serves the purpose of a numerical benchmark.

The ratio for response amplitudes for each model versus measured values can provide a rough estimate for model accuracy, where the values closer to 1 indicate a more accurate model. The TDSM and BKA-BEM methods, on average, generate values quite close to the measured response peaks. The subharmonic response peak value ratio (model to measured) are 1.3 to 1.6 on average for TDSM and BKA-BEM respectively. Furthermore, they have a similar level of accuracy in both the vertical and the horizontal response, which signifies robustness and stability of performance. The BEM model, on the other hand, has the best accuracy in the horizontal direction whereas in the vertical direction it shows the worst performance, with average subharmonic response peak value ratio of 0.9 and 5.9 respectively. The major contributor to the poor prediction in the vertical direction is the 4th subcritical harmonic response peak. This result shows that while the model has the ability to predict the dynamic behavior of the rotor very well in some cases, due to the direct relation between the harmonic excitation source (roundness or waviness) and the response (without the potential effect of bearing kinematics), any error or unusual correlation becomes highly amplified, which does not reflect the actual situation.

In terms of estimating the subcritical frequencies for the peaks, a comparison between each model and the measured peak frequencies shows that the three models have almost the same level of accuracy (± 0.2 variation on average). This finding indicates that the proposed models can comprehensively replicate the dynamic behavior of the system. However, in terms of amplitude estimation, the kinematics augmented model (BKA-BEM) shows more robustness and stability.

The developed methods perform relatively well compared to the measured response and the time domain solution with the benefit of being significantly lighter computationally. Based on this research and the test case, Table 5 presents the computational time using MATLAB 2019a.

Based on the results of this work, the authors propose the performance ratings in Table 6 for the two proposed frequency domain-based models in comparison with the high-fidelity model.

6. Conclusion

In this study, two frequency domain-based models are proposed that are able to account for excitations due to bearing roundness or waviness. The first method (BEM) considers the waviness as a base excitation, whereas the second method (BKA-BEM) utilizes a 4 DOF quasi-static model to augment the bearing kinematics and refine the base excitations due to waviness. The methods are validated with a test case where low order waviness or roundness of the inner ring is modified to obtain different subcritical vibration amplitudes. The performance of the developed methods was compared with experimental results as well as with a previously developed and validated detailed numerical model. The proposed frequency domain-based methods perform reasonably well with vastly improved computational efficiency compared to the well known time domain-based method. In terms of excitation frequency estimation, both proposed methods have highly accurate prediction and good stability. In terms of amplitude of response, both methods have fairly good accuracy, although the BKA-BEM has better stability and robustness.

6.1. Future work and application

The proposed methods can be developed further in the future for the following applications.

6.1.1. Design space exploration

For the design of a large or high-speed rotors, the rotordynamics behaviour is an important constraint, often based on which, other design parameters, such as supports and frame are selected [49]. In large rotors, the subcritical vibrations have significant effect on the overall vibration levels, for example in steel and paper industry applications. For such subcritical systems, bearing waviness, clearance [29] along with other bearing related faults can potentially create high subcritical resonances. Therefore, in early design phase, accounting for these sources of vibration is very important, preferably with a computationally efficient tool that does not extend the design engineering time. The BEM and BKA-BEM methods proposed in this study can be considered as a starting point of such a tool where the effect of waviness and clearance can be studied thoroughly along with sensitivity analysis. The BKA-BEM method can be further extended to make the bearing model more realistic and account for different bearing related defects and study their influence on the system.

Table 5
Approximate computational time for different models.

Models	Computing time (approx.)
TDSM (using 4 cores)	32344 seconds
BKA-BEM	5.4 seconds
BEM	2.6 seconds

Table 6
Comparison of the performance of the different models.

Models	Model complexity	Bearing nonlinear behavior	Computational speed	Accuracy	Robustness
TDSM	★★★★★	★★★★	★	★★★★	★★★★
BKA-BEM	★★★	★★★★	★★★	★★★★	★★★★
BEM	★★	★★	★★★★	★★★	★★

6.1.2. Input for dimensioning and tolerancing of bearings for specific applications

The algorithm can be used to determine the limits for roundness profiles and their influence to the system level behavior. Based on this assessment and allowable subcritical vibration levels, design engineers can specify the required surface finish and tolerances for the surfaces, and therefore design the rotor for the application. [50].

6.1.3. Iterative inverse identification and parameter estimation

In general, physics based models such as FE model used for representing machine behavior have uncertainties associated with them caused by unknown physical properties [51]. Some of these sources of modeling uncertainty can be parametrically identified by comparison with measured data. Specific to the method proposed in this study, bearing properties or support properties comprise of significant uncertainty levels. Using an inverse iteration and optimization approach [52] combined with measurements, these parameters can be identified.

6.1.4. Parallel real-time digital twins and condition monitoring

In recent years, researcher have used deep learning methods combined with frequency domain response, towards estimation of bearing remaining useful life (RUL) through feature extraction [53,54]. However, as Sobie et al. [55] observed, such intelligent models trained with experimental data tend to become case dependent. Furthermore, the training procedure has limitations in the form of availability of in-service data and lack of generalization. Therefore, instead of using experimental data set for training, a simulation model or digital twin [56] is arguably an inexpensive tool to take various failure mode scenarios into account or to analyze the dynamic behavior of a machine due to large scale parametric changes. The methods proposed in this study can be utilized to generate large training data and exploit transfer learning concepts [57].

CRediT authorship contribution statement

Tuhin Choudhury: Conceptualization, Methodology, Software, Investigation, Formal analysis, Writing - original draft, Writing - review & editing, Visualization, Validation. **Emil Kurvinen:** Software, Data curation, Investigation, Supervision, Funding acquisition, Project administration, Writing - original draft. **Raine Viitala:** Data curation, Investigation, Writing - original draft. **Jussi Sopanen:** Methodology, Funding acquisition, Project administration, Supervision, Software, Writing - original draft.

Declaration of competing interest

The authors declare that they have no known competing financial interests or personal relationships that could have appeared to influence the work reported in this paper.

Acknowledgement

This work was supported by Academy of Finland [Grant No. 313676].

References

[1] T.A. Harris, M.N. Kotzalas, Essential Concepts of Bearing Technology, CRC Press, 2006.
[2] G. Jang, S.-W. Jeong, Vibration analysis of a rotating system due to the effect of ball bearing waviness, J. Sound Vib. 269 (2004) 709–726, https://doi.org/10.1016/S0022-460X(03)00127-5.
[3] F. Wardle, Vibration forces produced by waviness of the rolling surfaces of thrust loaded ball bearings part 2: Experimental validation, Proc. Inst. Mech. Engrs, Part C: J. Mech. Eng. Sci. 202 (1988) 313–319, https://doi.org/10.1243/PIME_PROC_1988_202_128_02.
[4] F. Wardle, Vibration forces produced by waviness of the rolling surfaces of thrust loaded ball bearings part 1: Theory, Proc. Inst. Mech. Engrs, Part C: J. Mech. Eng. Sci. 202 (1988) 305–312, https://doi.org/10.1243/PIME_PROC_1988_202_127_02.

[5] W. Liu, Y. Zhang, Z.-J. Feng, J.-S. Zhao, D. Wang, A study on waviness induced vibration of ball bearings based on signal coherence theory, J. Sound Vib. 333 (2014) 6107–6120, https://doi.org/10.1016/j.jsv.2014.06.040.
[6] D.S. Shah, V. Patel, Theoretical and experimental vibration studies of lubricated deep groove ball bearings having surface waviness on its races, Measurement 129 (2018) 405–423, https://doi.org/10.1016/j.measurement.2018.07.031.
[7] C. Babu, N. Tandon, R. Pandey, Vibration modeling of a rigid rotor supported on the lubricated angular contact ball bearings considering six degrees of freedom and waviness on balls and races, J. Vib. Acoust. 134 (2012), https://doi.org/10.1115/1.4005140.
[8] C. Babu, N. Tandon, R. Pandey, Nonlinear vibration analysis of an elastic rotor supported on angular contact ball bearings considering six degrees of freedom and waviness on balls and races, J. Vib. Acoust. 136 (2014), https://doi.org/10.1115/1.4027712.
[9] S. Adamczak, P. Zmarzły, Influence of raceway waviness on the level of vibration in rolling-element bearings, Bull. Pol. Acad. Sci. Techn. Sci. 65 (2017), https://doi.org/10.1515/bpasts-2017-0059.
[10] D.J. Inman, Engineering Vibration, volume 3, 3rd ed., Prentice Hall Englewood Cliffs, NJ, 2007.
[11] S. Harsha, K. Sandeep, R. Prakash, Non-linear dynamic behaviors of rolling element bearings due to surface waviness, J. Sound Vib. 272 (2004) 557–580, https://doi.org/10.1016/S0022-460X(03)00384-5.
[12] M. Cao, J. Xiao, A comprehensive dynamic model of double-row spherical roller bearing–model development and case studies on surface defects, preloads, and radial clearance, Mech. Syst. Sig. Process. 22 (2008) 467–489, https://doi.org/10.1016/j.ymssp.2007.07.007.
[13] J. Sopanen, A. Mikkola, Dynamic model of a deep-groove ball bearing including localized and distributed defects. part 1: Theory, Proc. Inst. Mech. Engr., Part K: J. Multi-body Dyn. 217 (2003) 201–211. doi: 10.1243/14644190360713551.
[14] J. Sopanen, A. Mikkola, Dynamic model of a deep-groove ball bearing including localized and distributed defects. part 2: Implementation and results, Proc. Inst. Mech. Engr., Part K: J. Multi-body Dyn. 217 (2003) 213–223. doi: 10.1243/14644190360713560.
[15] R. Liu, X. Xiong, C. Zhou, Effects of raceway waviness on dynamic behaviors of deep groove ball bearing, in: IOP Conference Series: Materials Science and Engineering, volume 493, IOP Publishing, 2019, p. 012052. doi: 10.1088/1757-899x/493/1/012052.
[16] L. Niu, A simulation study on the effects of race surface waviness on cage dynamics in high-speed ball bearings, J. Tribol. 141 (2019), https://doi.org/10.1115/1.4042656.
[17] H. Wang, Q. Han, D. Zhou, Nonlinear dynamic modeling of rotor system supported by angular contact ball bearings, Mech. Syst. Sig. Process. 85 (2017) 16–40, https://doi.org/10.1016/j.ymssp.2016.07.049.
[18] X. Wang, Q. Xu, M. Huang, L. Zhang, Z. Peng, Effects of journal rotation and surface waviness on the dynamic performance of aerostatic journal bearings, Tribol. Int. 112 (2017) 1–9, https://doi.org/10.1016/j.triboint.2017.03.027.
[19] J. Liu, Y. Shao, Vibration modelling of nonuniform surface waviness in a lubricated roller bearing, J. Vib. Control 23 (2017) 1115–1132, https://doi.org/10.1177/1077546315589675.
[20] S.P. Patel, S. Upadhyay, Influence of roller defect and coupled roller–inner–outer race defects on the performance of cylindrical roller bearing, Proc. Inst. Mech. Engrs., Part K: J. Multi-body Dyn. 233 (2019) 731–746. doi: 10.1177/1464419318819332.
[21] X. Zhang, Q. Han, Z. Peng, F. Chu, Stability analysis of a rotor–bearing system with time-varying bearing stiffness due to finite number of balls and unbalanced force, J. Sound Vib. 332 (2013) 6768–6784, https://doi.org/10.1016/j.jsv.2013.08.002.
[22] X. Zhang, Q. Han, Z. Peng, F. Chu, A comprehensive dynamic model to investigate the stability problems of the rotor–bearing system due to multiple excitations, Mech. Syst. Sig. Process. 70 (2016) 1171–1192, https://doi.org/10.1016/j.ymssp.2015.10.006.
[23] N. Aktürk, The effect of waviness on vibrations associated with ball bearings, J. Tribol. 121 (1999) 667–677, https://doi.org/10.1115/1.2834121.
[24] G. Jang, S. Jeong, Nonlinear excitation model of ball bearing waviness in a rigid rotor supported by two or more ball bearings considering five degrees of freedom, J. Tribol. 124 (2002) 82–90, https://doi.org/10.1115/1.1398289.
[25] S. Harsha, P. Kankar, Stability analysis of a rotor bearing system due to surface waviness and number of balls, Int. J. Mech. Sci. 46 (2004) 1057–1081, https://doi.org/10.1016/j.ijmecsci.2004.07.007.
[26] S. Harsha, K. Sandeep, R. Prakash, Nonlinear dynamic response of a rotor bearing system due to surface waviness, Nonlinear Dyn. 37 (2004) 91–114, https://doi.org/10.1023/B:NODY.0000042916.10351.ff.
[27] R. Viitala, T. Widmaier, P. Kuosmanen, Subcritical vibrations of a large flexible rotor efficiently reduced by modifying the bearing inner ring roundness profile, Mech. Syst. Sig. Process. 110 (2018) 42–58, https://doi.org/10.1016/j.ymssp.2018.03.010.
[28] J.E. Heikkinen, B. Ghalamchi, R. Viitala, J. Sopanen, J. Juhanko, A. Mikkola, P. Kuosmanen, Vibration analysis of paper machine's asymmetric tube roll supported by spherical roller bearings, Mech. Syst. Sig. Process. 104 (2018) 688–704, https://doi.org/10.1016/j.ymssp.2017.11.030.
[29] E. Kurvinen, R. Viitala, T. Choudhury, J. Heikkinen, J. Sopanen, Simulation of subcritical vibrations of a large flexible rotor with varying spherical roller bearing clearance and roundness profiles, Machines 8 (2020) 28, https://doi.org/10.3390/machines8020028.
[30] R.B. Randall, J. Antoni, Rolling element bearing diagnostics–a tutorial, Mech. Syst. Sig. Process. 25 (2011) 485–520, https://doi.org/10.1016/j.ymssp.2010.07.017.
[31] S. Harsha, K. Sandeep, R. Prakash, The effect of speed of balanced rotor on nonlinear vibrations associated with ball bearings, Int. J. Mech. Sci. 45 (2003) 725–740, https://doi.org/10.1016/S0020-7403(03)00064-X.
[32] S. Saito, Calculation of nonlinear unbalance response of horizontal jeffcott rotors supported by ball bearings with radial clearances, J. Vib. Acoust. Stress Reliab. Des. 107 (1985) 416–420, https://doi.org/10.1115/1.3269282.
[33] K. Ono, Y. Okada, Analysis of ball bearing vibrations caused by outer race waviness, J. Vib. Acoust. 120 (1998) 901–908, https://doi.org/10.1115/1.2893918.
[34] T. Tiainen, J. Miettinen, R. Viitala, K. Hiekkanen, P. Kuosmanen, Digital twin and virtual sensor for a rotor system, Ann. DAAAM Proc. 30 (2019).
[35] R.L. Ruhl, J.F. Booker, A finite element model for distributed parameter turborotor systems, J. Eng. Ind. 94 (1972) 126–132, https://doi.org/10.1115/1.3428101.
[36] W.J. Chen, E.J. Gunter, et al., Introduction to Dynamics of Rotor-Bearing Systems, volume 175, Trafford Victoria, 2007.
[37] H.D. Nelson, J.M. McVaugh, The dynamics of rotor-bearing systems using finite elements, J. Eng. Ind. 98 (1976) 593–600, https://doi.org/10.1115/1.3438942.
[38] E. Kurvinen, J. Sopanen, A. Mikkola, Ball bearing model performance on various sized rotors with and without centrifugal and gyroscopic forces, Mech. Mach. Theory 90 (2015) 240–260, https://doi.org/10.1016/j.mechmachtheory.2015.03.017.
[39] B. Ghalamchi, J. Sopanen, A. Mikkola, Simple and versatile dynamic model of spherical roller bearing, Int. J. Rotating Mach. 2013 (2013), https://doi.org/10.1155/2013/567542.
[40] G. Dormond, Modal identification and modeling of bearings for very high-speed rotors, Technical Report, EPFL, 2010.
[41] E. Krämer, Rotor and foundation, Springer, 1993.
[42] T. Widmaier, B. Hemming, J. Juhanko, P. Kuosmanen, V.-P. Esala, A. Lassila, P. Laukkanen, J. Haikio, Application of monte carlo simulation for estimation of uncertainty of four-point roundness measurements of rolls, Prec. Eng. 48 (2017) 181–190, https://doi.org/10.1016/j.precisioneng.2016.12.001.
[43] P. McFadden, A revised model for the extraction of periodic waveforms by time domain averaging, Mech. Syst. Sig. Process. 1 (1987) 83–95, https://doi.org/10.1016/0888-3270(87)90085-9.
[44] H. Nelson, A finite rotating shaft element using timoshenko beam theory, J. Mech. Des. 102 (1980) 793–803, https://doi.org/10.1115/1.3254824.
[45] K. Cavalca, P. Cavalcante, E. Okabe, An investigation on the influence of the supporting structure on the dynamics of the rotor system, Mech. Syst. Sig. Process. 19 (2005) 157–174, https://doi.org/10.1016/j.ymssp.2004.04.001.
[46] R. Viitala, R. Viitala, Method and device to investigate the behavior of large rotors under continuously adjustable foundation stiffness, J. Vibroeng. 22 (2020) 1037–1054, https://doi.org/10.21595/jve.2020.21107.
[47] J. Juhanko, E. Porkka, T. Widmaier, P. Kuosmanen, Dynamic geometry of a rotating cylinder with shell thickness variation, Est. J. Eng. 16 (2010) 285, https://doi.org/10.3176/eng.2010.4.04.
[48] L. Meirovitch, Fundamentals of vibrations, Waveland Press, 2010.

[49] N. Uzhegov, E. Kurvinen, J. Nerg, J. Pyrhönen, J.T. Sopanen, S. Shirinskii, Multidisciplinary design process of a 6-slot 2-pole high-speed permanent-magnet synchronous machine, IEEE Trans. Industr. Electron. 63 (2016) 784–795, https://doi.org/10.1109/TIE.2015.2477797.
[50] R. Viitala, Minimizing the bearing inner ring roundness error with installation shaft 3d grinding to reduce rotor subcritical response, CIRP J. Manuf. Sci. Technol. 30 (2020) 140–148, https://doi.org/10.1016/j.cirpj.2020.05.002.
[51] R. Pasquier, I.F. Smith, Iterative structural identification framework for evaluation of existing structures, Eng. Struct. 106 (2016) 179–194, https://doi.org/10.1016/j.engstruct.2015.09.039.
[52] C. Ding, M. Zhao, J. Lin, J. Jiao, Multi-objective iterative optimization algorithm based optimal wavelet filter selection for multi-fault diagnosis of rolling element bearings, ISA Trans. 88 (2019) 199–215, https://doi.org/10.1016/j.isatra.2018.12.010.
[53] L. Ren, J. Cui, Y. Sun, X. Cheng, Multi-bearing remaining useful life collaborative prediction: A deep learning approach, J. Manuf. Syst. 43 (2017) 248–256, https://doi.org/10.1016/j.jmsy.2017.02.013.
[54] O. Janssens, V. Slavkovikj, B. Vervisch, K. Stockman, M. Loccufier, S. Verstockt, R. Van de Walle, S. Van Hoecke, Convolutional neural network based fault detection for rotating machinery, J. Sound Vib. 377 (2016) 331–345, https://doi.org/10.1016/j.jsv.2016.05.027.
[55] C. Sobie, C. Freitas, M. Nicolai, Simulation-driven machine learning: Bearing fault classification, Mech. Syst. Sig. Process. 99 (2018) 403–419, https://doi.org/10.1016/j.ymssp.2017.06.025.
[56] E.J. Tuegel, A.R. Ingraffea, T.G. Eason, S.M. Spottswood, Reengineering aircraft structural life prediction using a digital twin, Int. J. Aerosp. Eng. 2011 (2011), https://doi.org/10.1155/2011/154798.
[57] Y. Lei, B. Yang, X. Jiang, F. Jia, N. Li, A.K. Nandi, Applications of machine learning to machine fault diagnosis: A review and roadmap, Mech. Syst. Sig. Process. 138 (2020), 106587.